Broadband Spin-Selective Wavefront Manipulations Based on Pancharatnam−Berry Coding Metasurfaces

Yue Gou, Hui Feng Ma,* Liang Wei Wu, Zheng Xing Wang, Peng Xu, and Tie Jun Cui*

ACCESS | Metrics & More | Article Recommendations

ABSTRACT: Spin-selective reflection metadevices are usually realized by using chiral metamirrors that can reflect one state of circularly polarized (CP) waves and restrain the other one. However, most of the chiral metamirrors only exhibit chirality in a narrow band, which may impede their potential applications. Here, we propose a Pancharatnam−Berry (PB) coding metasurface composed of the spin-decoupled elements to realize broadband spin-selective reflections with arbitrary wavefront manipulations. The spin-selective anomalous reflection is designed and measured to validate the performance of the proposed PB coding metasurface. Both simulation and experiment results show that the designated CP wave can be efficiently reflected without reversing the spin state, while at the same time, its orthogonally polarized wave is suppressed by random diffusion, in a broad band from 16 to 24 GHz. The results also reveal that the proposed PB coding metasurface has the chiral-like characteristics, even though it is composed of nonchiral meta-elements.
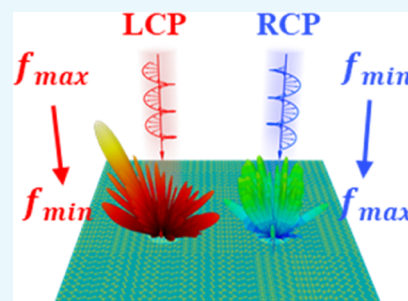
1. INTRODUCTION

Metasurfaces are composed of two-dimensional (2D) sub-wavelength artificial elements and have attracted much attention in recent years due to their powerful ability in the manipulations of electromagnetic (EM) waves.[1−4] However, most of the traditional metasurfaces have no chirality, and thus they have the same amplitude and/or phase responses for both left- and right-handed circularly polarized (CP) waves.[5,6] The proposal of Pancharatnam−Berry (PB) metasurfaces makes it possible to control the left- and right-handed CP waves independently because the introduction of the propagation and geometric phases can break the locked spin-flipped phase limitation.[7−9] Many fantastic works have been proposed on the basis of PB metasurfaces, such as the broadband spin-decoupled reflector antenna,[10] multichannel vectorial holo-gram,[11−13] multiple-input multiple-output antenna with information encryption,[14] near-field and far-field optical imaging,[15,16] polarization-insensitive cloaking,[17] and even helicity-delinked manipulations of surface waves.[18]

Chiral metamirrors as a special kind of metasurface,[19,20] which can efficiently reflect the designated CP waves without reversing the spin state and simultaneously suppress its orthogonally polarized wave by absorption, have also attracted much attention. They are widely used in the spin-selective wavefront manipulation of EM waves, such as the spin-selective anomalous reflection,[21,22] chiral multiplexing holo-gram,[23] dual-band spin-selective absorber,[24] and full-dimen-sional manipulation of optical waves.[25] However, the previous chiral metamirrors are generally based on asymmetric resonant elements, which must meet the requirement of breaking n-fold ($n > 2$) rotational symmetries, and most of them can only

exhibit chiral response in a narrow band. Reference 26 proposes that combining two asymmetric split-ring resonators into a supercell can increase a certain bandwidth of chiral response, whose full width at half maximum is 5.7%. Nevertheless, the absorption of such a supercell-based chiral metamirror is still attributed to the spin-selective induced resonance within the chiral elements, which leads to the limitation of absorption bandwidth.

Digital coding metasurfaces as a bridge linking between the physics world and digital information world has attracted much attention in recent years,[27] which opens up a new avenue for the development of metasurfaces. In addition to the control of linearly polarized waves,[28−36] the digital coding metasurfaces can also be used for the manipulation of CP waves, such as the multiple beams control,[37] spin-to-orbital generation,[38] spin-symmetry breaking,[39] and even quantum information representation.[40] However, most of the previous works only focus on simultaneously manipulating the wavefronts of left-handed and right-handed CP waves with the same reflection efficiency and a lack of discussion about spin-selective reflection, which may find some potential applications similar to the chiral materials, but having an obvious advantage in broad bandwidth.
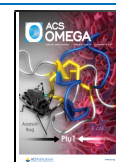
In this paper, a new method based on the spin-decoupled PB coding metasurface has been proposed to achieve the broadband spin-selective wavefront manipulation. Different from the traditional chiral metamirror that is composed of chiral meta-elements, the proposed PB metasurface is composed of 2-bit coding nonchiral elements. By introducing both the geometric phase and propagation phase, the wavefront of left-handed CP (LCP) and right-handed CP (RCP) waves can be manipulated independently without reversing spin states. Hence, the spin-selective reflection with the arbitrary wavefront manipulation can be achieved by efficiently reflecting the designated CP wave (LCP or RCP wave) and at the same time randomly diffusing its orthogonal polarized wave (RCP or LCP wave). More importantly, because no resonant chiral meta-elements are used in this design, therefore the proposed spin-selective PB metasurfaces can work in a broad frequency band. A PB coding metasurface with the spin-selective anomalous reflection has been designed and measured, and the results show that the proposed PB coding metasurface has a good spin-selective performance in a broad band from 16 to 24 GHz. Meanwhile, the results also show that the proposed spin-selective PB coding metasurface also has the chiral-like characteristics, even though it is composed of nonchiral elements.

2. RESULTS AND DISCUSSION

2.1. Theoretical Analysis and Simulations.
The schematic of the proposed PB coding metasurface is demonstrated in Figure 1a, which has the ability to
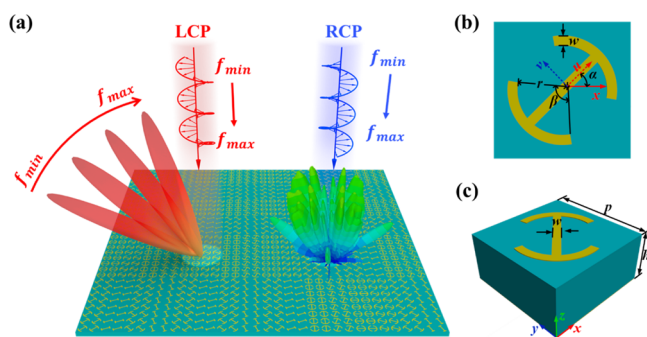
Figure 1. Schematic of the EM responses of the proposed PB coding metasurface and its unit structure. (a) Metasurface can anomalously reflect the LCP wave without reversing the handedness, while suppressing the RCP waves by random diffusion in a broad frequency band. (b,c) Quasi-I-shaped structure.

anomalously reflect the designated CP wave without reversing the handedness, while simultaneously suppressing its orthogonal spin state. We arbitrarily assume that the LCP wave is efficiently reflected, while the RCP wave is suppressed by random diffusion.

The metasurface is composed of quasi-I-shaped structures, as demonstrated in Figure 1b,c, which is designed based on the printed circuit board technology. The thickness of covered copper is 0.018 mm with conductivity of 5.8×10^7 s/m. A grounded plane is on the back of the unit structure spaced by a dielectric substrate of F4BK265 (polytetrafluoroethylene) with thickness of $h = 2$ mm, whose relative permittivity is 2.65 and loss tangent is 0.001. The other parameters shown in Figure 1b,c are $P = 4.4$ mm, $w = 0.32$ mm, $r = 1.75$ mm, and variables α and β, where α is defined as the azimuth angle along the x

axis and β is defined as the angle of arc. In order to more easily show the performance of the unit structure, a new local coordinate is defined as uov, in which the axes u and v are parallel and vertical, respectively, to the metallic strip connected to two arcs.

Figure 2 shows the phase and amplitude responses of the unit varying with α and β, which are simulated by using commercial software CST Microwave Studio (CST Computer Simulation Technology GmbH, Darmstadt, Germany). The phase difference between the u- and v-polarized reflection waves can keep 180° in a broad band for any β, such as $\beta = 48$, 92, 124, and 154°, as shown in Figure 2a, implying that the unit structures satisfy the requirement of PB phase. It is worth mentioning that the unit cell boundary condition is adopted in all simulations, as the inset shown in Figure 2b, while the plane wave excitation can be set as linearly and circularly polarized waves, respectively, according to the requirements. The reflection phases of CP waves varying with β at different frequencies are demonstrated in Figure 2c, in which α is fixed as 0°. The results show that the reflection phases are almost linearly decreased as β increases, and this β-dependent reflection phase (φ_β) is usually named as the propagation phase. The reflection phases of CP waves varying with α at different frequencies are demonstrated in Figure 2e, in which β is fixed as 154°. The results show that the reflection phases are gradually increased for LCP waves and decreased for RCP waves as α increases, and this α-dependent reflection phase (φ_α) is usually named as the geometric phase. In addition, the units can keep high reflection efficiency for the different cases as shown in Figure 2b–f.

In order to obtain the reflection phases of LCP and RCP waves, it can start from the relationship between the incident waves and reflection waves under the xoy coordinate when the unit structure is rotated by an angle of α, which can be expressed as

$$\begin{bmatrix} E_x^r \\ E_y^r \end{bmatrix} = MRM^{-1} \begin{bmatrix} E_x^i \\ E_y^i \end{bmatrix}$$

(1)

in which E_x^r and E_y^r represent the x- and y-polarized components of the reflected waves, E_x^i and E_y^i represent the x- and y-polarized components of the incident waves, $\mathbf{M} = \begin{bmatrix} \cos \alpha & -\sin \alpha \\ \sin \alpha & \cos \alpha \end{bmatrix}$ is the rotation matrix, and $\mathbf{R} = \begin{bmatrix} A_u \, e^{i\varphi_u} & 0 \\ 0 & A_v \, e^{i\varphi_v} \end{bmatrix}$ is the reflection matrix of the unit structure under the uov coordinate; here $A_u = A_v = 1$ because all the incident waves are almost totally reflected, and $\varphi_v - \varphi_u \approx \pi$ according to the results shown in Figure 2a. The LCP and RCP components can be expressed with the linear polarization components under the xoy coordinate by

$$\begin{bmatrix} E_L^i \\ E_R^i \end{bmatrix} = \frac{1}{\sqrt{2}} \begin{bmatrix} 1 & i \\ 1 & -i \end{bmatrix} \begin{bmatrix} E_x^i \\ E_y^i \end{bmatrix}$$

$$\begin{bmatrix} E_{LL}^r \\ E_{RR}^r \end{bmatrix} = \frac{1}{\sqrt{2}} \begin{bmatrix} 1 & -i \\ 1 & i \end{bmatrix} \begin{bmatrix} E_x^r \\ E_y^r \end{bmatrix}$$

(2)

in which E_L^i and E_R^i represent the LCP and RCP components of the incident waves, and E_{LL}^r and E_{RR}^r represent the LCP and RCP components of the reflected waves. It is worth
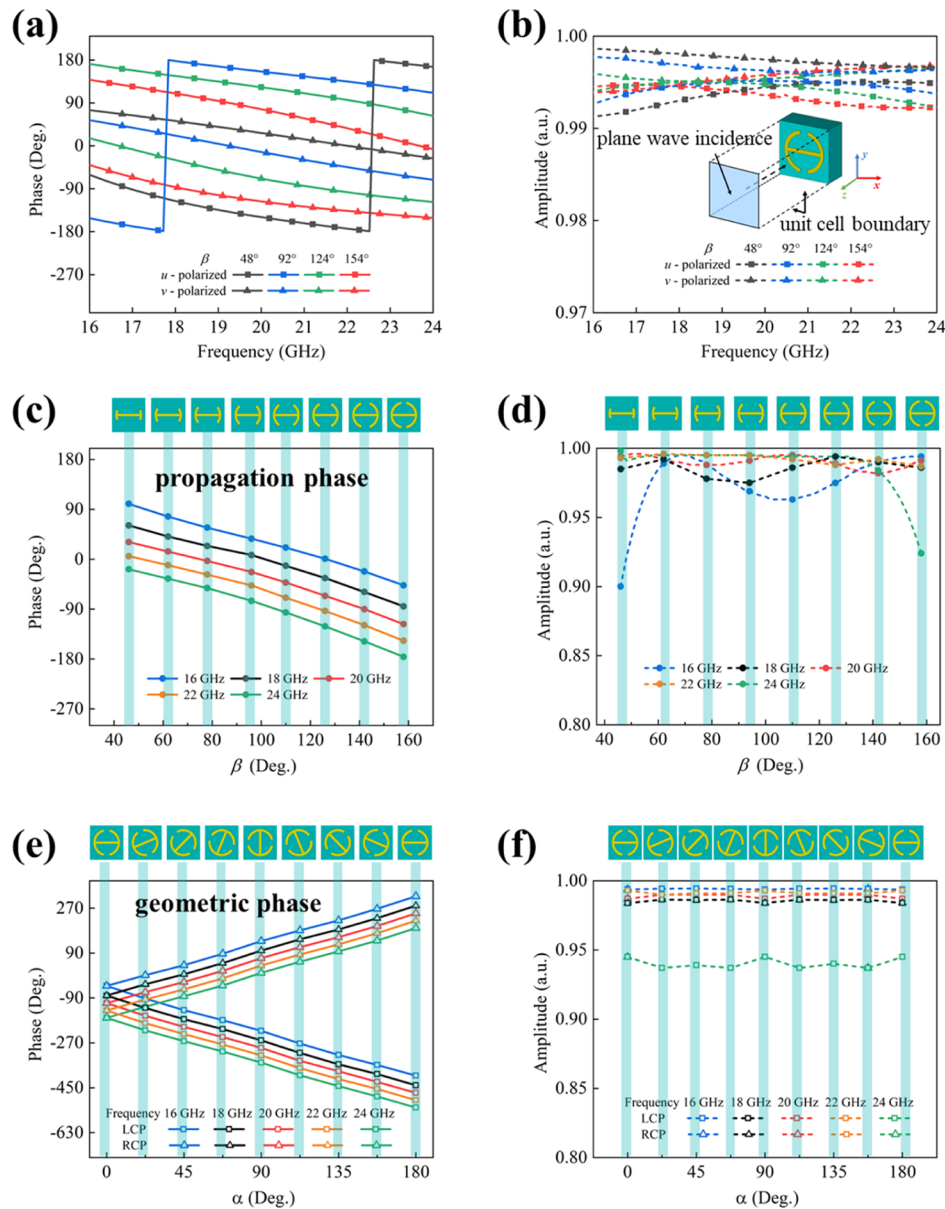
Figure 2. EM responses of the unit element. (a,b) Simulated reflection phase and amplitude responses of the element for u- and v-polarized waves with β = 48, 92, 124, and 154° from 16 to 24 GHz. (c,d) Simulated reflection phase and amplitude responses of the element for CP waves with different β at 16, 18, 20, 22, and 24 GHz, with α fixed to be 0°. (e,f) Simulated reflection phase and amplitude responses of the element for LCP and RCP waves with different α at 16, 18, 20, 22, and 24 GHz, with β fixed to be 154°.

mentioning that the LCP (and RCP) waves have the opposite rotation direction for the incident and reflected LCP (and RCP) waves because their transmission directions are also opposite. We define $C = \frac{1}{\sqrt{2}}\begin{bmatrix} 1 & i \\ 1 & -i \end{bmatrix}$ and $C' = \frac{1}{\sqrt{2}}\begin{bmatrix} 1 & -i \\ 1 & i \end{bmatrix}$, then combining eqs 1 and 2, there is

$$\begin{bmatrix} E_{LL}^r \\ E_{RR}^r \end{bmatrix} = C'MRM^{-1}C^{-1}\begin{bmatrix} E_L^i \\ E_R^i \end{bmatrix} = \begin{bmatrix} e^{i(\varphi_u - 2\alpha)} & 0 \\ 0 & e^{i(\varphi_u + 2\alpha)} \end{bmatrix}\begin{bmatrix} E_L^i \\ E_R^i \end{bmatrix} \quad (3)$$

Therefore, the reflection phases of LCP and RCP waves can be calculated by

$$\begin{cases} \varphi_{LL} = \varphi_u - 2\alpha = \varphi_\beta - 2\alpha \\ \varphi_{RR} = \varphi_u + 2\alpha = \varphi_\beta + 2\alpha \end{cases} \quad (4)$$

in which $\varphi_u = \varphi_\beta$ is the propagation phase and $\varphi_\alpha = 2\alpha$ is the geometric phase. Hence, according to eq 4, the PB metasurfaces can independently control the reflection phases of LCP and RCP waves by changing α and β.

Four different unit structures with β = 154, 124, 92, and 48° are selected to construct the 2-bit PB coding metasurface, whose propagation phases continuously increase with the interval of about 45° when β decreases from 154 to 48°, as shown in Figure 2c. We note that the absolute phase values of these units will not affect the performance of the PB coding metasurface and therefore can be normalized to the reflection phase of digital code "00" (0°), which is an unit with β = 154° and α = 0. Then, the other spin-decoupled digital codes "01" (90°), "10" (180°), and "11" (270°) for both LCP and RCP waves can be achieved according to the eq 2. At last, 16 unit elements are used to construct the proposed PB coding

Figure 3. 2-bit spin-decoupled unit coding elements.

Figure 4. Characterization of the L-type gradient coding metasurface with the broadband spin-selective reflection. (a) Phase distributions for LCP and RCP waves and layout of the metamirror. (b,c) Full-wave simulated 2D and 3D (insets) far-field radiation patterns of the metamirror under the normal incidence of (b) LCP and (c) RCP waves.

metasurface, as demonstrated in Figure 3. For simplicity, these units are named as "C_L/C_R", in which C_L and C_R represent the digital states of LCP and RCP waves, respectively.

A 2-bit PB coding metasurface with the function of spin-selective anomalous reflection is designed and simulated by encoding the gradient phase code of LCP wave and the random phase code of RCP wave into a single metasurface, as shown in Figure 4a. The gradient phase coding pattern comprises eight phase periods along x direction with the

coding sequence of "00, 00, 01, 01, 10, 10, 11, 11". The random phase coding pattern contains 8 × 8 equal-sized blocks and each block is composed of 4 × 4 1-bit unit cells of "00" or "10". Hence, eight unit elements of "00/00", "00/10", "01/00", "01/10", "10/00", "10/10", "11/00", and "11/10" are used to construct the PB coding metasurface, as shown in Figure 4a, named as an L-type metasurface, which is composed of 32 × 32 pixels with an area of 140.8 × 140.8 mm². According to the
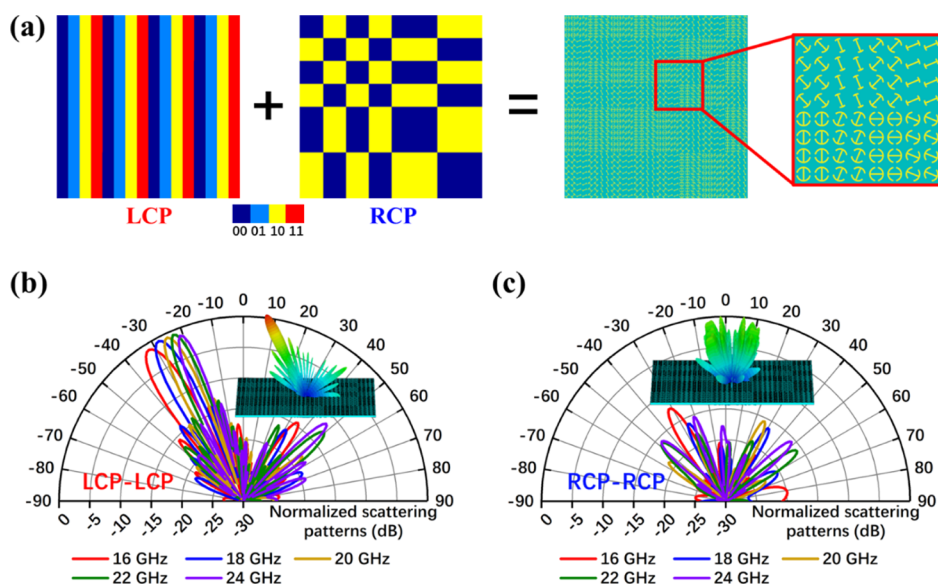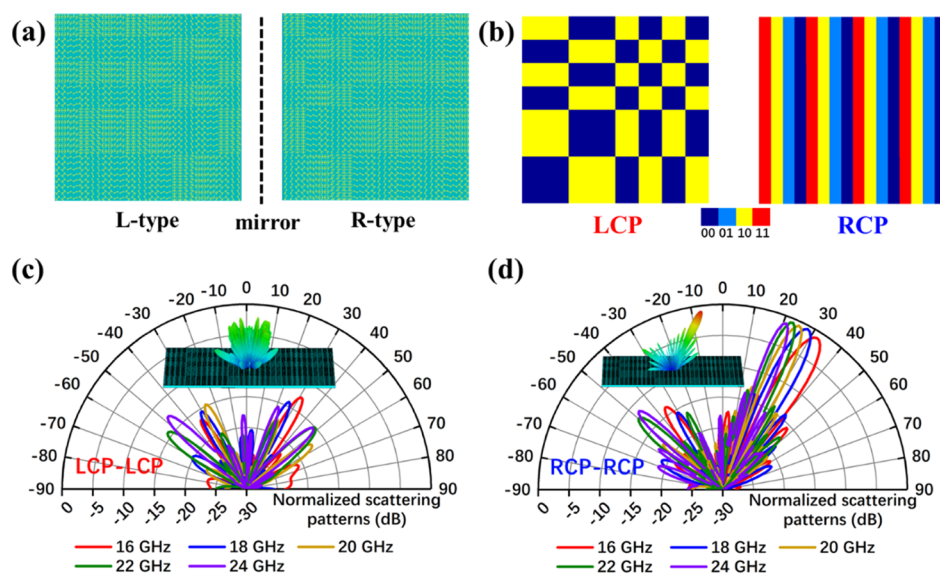
Figure 5. Characterization of the R-type gradient coding metasurface with broadband spin-selective reflection. (a) Layout of the L-type and R-type metasurfaces. (b) Phase distributions of the R-type metasurface for LCP and RCP waves. (c,d) Full-wave simulated 2D and 3D (insets) far-field radiation patterns under the normal incidence of (c) LCP and (d) RCP waves.
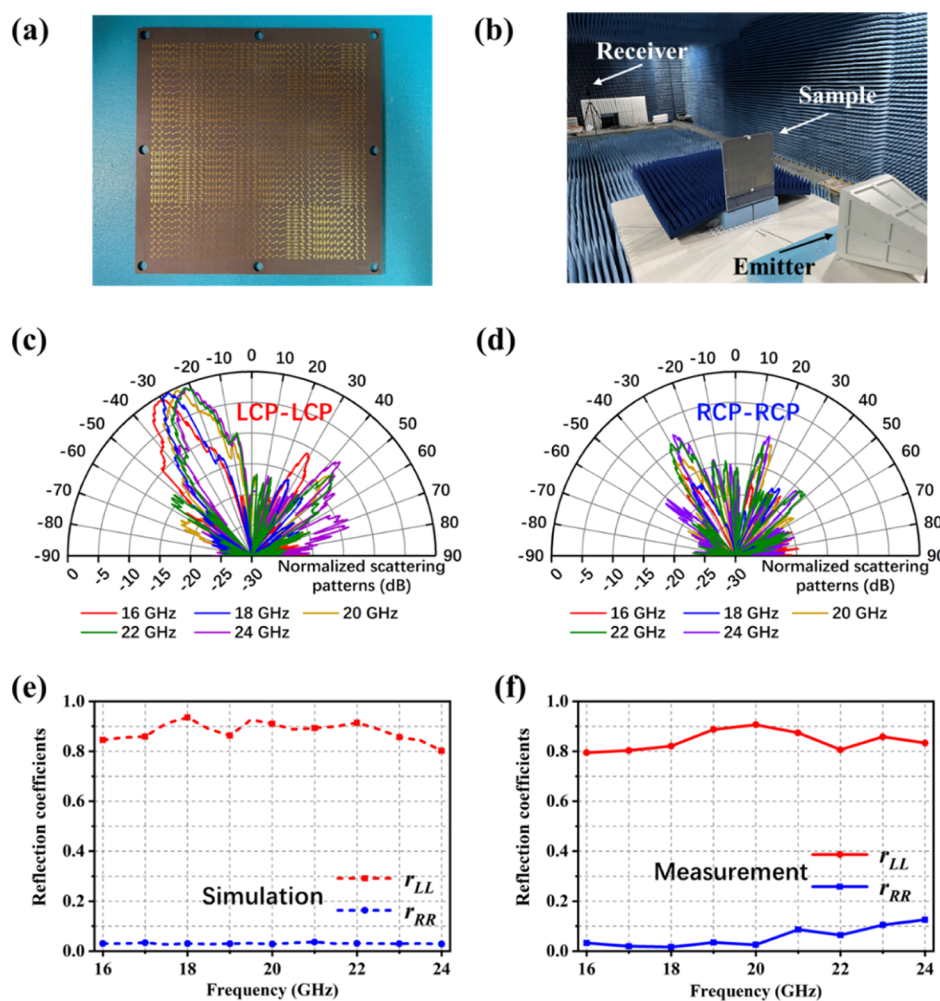
Figure 6. Experimental setup and measurement results. (a) Photograph of the fabricated prototype of L-type gradient coding chiral metamirror. (b) Experimental setup in an anechoic chamber. (c,d) Measured far-field radiation patterns at different frequencies for (c) LCP and (d) RCP waves, respectively. (e,f) Co-polarization reflection coefficients for LCP and RCP as a function of frequency. (e) Simulation and (f) measurement.

knowledge of general Snell's law,[1] the angle of the anomalous reflection waves can be calculated by

$$\theta_r = \sin^{-1}(\sin\theta_i + \lambda_0/\Gamma) \qquad (5)$$

in which θ_r is the reflection angle, θ_i is the incident angle, λ_0 is the working wavelength, and Γ is the physical length of one 2π phase period. In this design, θ_i is equal to 0 ($\theta_i = 0$) due to the normal incidence and $\Gamma = 8 \times p = 35.2$ mm; therefore, the reflection angle is only related to the working wavelength of λ_0. Figure 4b,c shows the full-wave simulated far-field radiation patterns at different frequencies in the *xoz* plane, in which Figure 4b shows the results of LCP wave and Figure 4c shows the results of RCP wave, and the results are normalized by the reflection energy of a bare copper plate with the same dimension. The insets demonstrate the three-dimensional (3D) far-field radiation patterns of the metasurface at 20 GHz. The results show that the RCP waves are randomly diffused to achieve low RCS scattering, which are smaller than −12 dB at different frequencies. It is worth mentioning that the large sidelobes shown in Figure 4b are mainly caused by the large discrete phase distribution of 2-bit coding sequence, which may be improved by using a higher bit coding sequence with a more continuous phase distribution. Although the LCP waves are anomalously reflected with high efficiency, whose reflection angles are −32, −28, −25, −23, and −20° at 16, 18, 20, 22, and 24 GHz, respectively, having a good agreement with the theoretical expectation.

Figure 5a shows the mirror of L-type metasurface, called as a R-type metasurface, whose phase coding patterns are mirrored with that of the L-type metasurface, as shown in Figure 5b. The full-wave simulation results of the R-type metasurface are demonstrated in Figure 5c,d, which shows that it has the completely opposite EM responses to that of the L-type metasurface. The LCP wave is suppressed by random diffusion, while the RCP wave is efficiently reflected with radiation angles of 32, 28, 25, 23, and 20° at 16, 18, 20, 22, and 24 GHz, respectively. It should be noted that the L-type and R-type metasurfaces cannot be coincided with each other through translation or rotation operation; therefore, the proposed PB coding metasurface also exhibits the chiral-like characteristics, even though it is not composed of chiral elements.

2.2. Experimental Results. The L-type PB coding metasurface has been fabricated, as shown in Figure 6a, and measured in an anechoic chamber, as shown in Figure 6b. A pair of CP horns are used for emitting and receiving the signals, in which the emitting horn and the metasurface are placed on a rotating platform with a distance about 60 cm to make sure that the incident waves are plane waves and normally illuminate the metasurface, while the receiving horn is placed in the other side of the anechoic chamber to receive the reflected signals, and the distance between the sample and receiver is about 9 m to satisfy the far-field measurement condition. It is worth mentioning that the emitting horn and receiving horn have the same polarization property, that is, the emitting signal and receiving signal have the same spin state. The measured far-field radiation patterns of LCP and RCP waves are demonstrated in Figure 6c,d, respectively, which are normalized to the reflection power generated by the bare copper plate with the same size. The results show that the LCP waves are efficiently reflected without reversing the polarization state, whose reflection angles are −31.9, −28.8, −24.5, −23.3, and −22.8° at 16, 18, 20, 22, and 24 GHz, respectively. While the RCP waves are randomly diffused, achieving a low

RCS scattering in a broad frequency band from 16 to 24 GHz. The measured results are basically consistent very well with the simulation results shown in Figure 4b,c except for some slight deviation, which are mainly caused by the errors of fabrication and measurement. Figure 6e,f shows the simulated and measured reflection coefficients of the L-type PB coding metasurface, which are obtained by normalizing the reflection energy of the metasurface to that of a bare copper plate with the same size. The results show that the reflection efficiency of the main beam of LCP waves can be as high as 80% from 16 to 24 GHz, while the RCP waves are strongly suppressed with reflection coefficient less than 10%. The measured results show a good agreement with the simulations, validating that the proposed PB coding metasurface exhibits a broadband spin-selective reflection characteristic. In addition, the performance of the proposed PB coding metasurface compared to the existing works in terms of the bandwidth is illustrated in Table 1, which further shows that the proposed PB coding metasurface has an obvious advantage in a ultra-wide spin-selective frequency band, with relative bandwidth up to 30%.

Table 1. Comparison of Bandwidth Performance between the Existing Works and This Design

	relative bandwidth
ref 19	single frequency@5.65 GHz
ref 20	single frequency@37.0 THz
ref 21	single frequency@9.00 GHz
ref 22	single frequency@9.50 GHz
ref 23	single frequency@0.60 THz
ref 24	dual frequencies@12.1 GHz and 14.4 GHz
ref 26	5.1% (9.89−10.41 GHz)
this work	30% (16−24 GHz)

3. CONCLUSIONS

We propose a PB coding metasurface that is composed of spin-decoupled coding elements. By elaborately designing the coding phase distributions of the metasurface, the broadband spin-selective reflection with the arbitrary wavefront manipulation can be realized in the microwave regime. In addition, the results show that the PB coding metasurface also has the chiral-like characteristics, even though it is constructed by the nonchiral spin-decoupled elements, which is because the PB coding metasurface composed of these nonchiral spin-decoupled elements exhibits the characteristics of breaking both the *n*-fold ($n > 2$) rotational and mirror symmetries. Both simulated and measured results validate the broadband characteristic of the proposed PB coding metasurface in the spin-selective wavefront manipulation. Compared with the conventional chiral metamirrors that are based on the asymmetric resonant structures, the proposed work opens up a new avenue for realizing the broadband spin-selective devices.

■ AUTHOR INFORMATION

Corresponding Authors

Hui Feng Ma − *State Key Laboratory of Millimeter Waves, School of Information Science and Engineering, Southeast University, Nanjing 210096, China;* ⊙ orcid.org/0000-0001-9315-9915; Email: hfma@seu.edu.cn

Tie Jun Cui − *State Key Laboratory of Millimeter Waves, School of Information Science and Engineering, Southeast*

University, Nanjing 210096, China; ⊙ orcid.org/0000-0002-5862-1497; Email: tjcui@seu.edu.cn

Authors

Yue Gou − *State Key Laboratory of Millimeter Waves, School of Information Science and Engineering, Southeast University, Nanjing 210096, China*

Liang Wei Wu − *State Key Laboratory of Millimeter Waves, School of Information Science and Engineering, Southeast University, Nanjing 210096, China*

Zheng Xing Wang − *State Key Laboratory of Millimeter Waves, School of Information Science and Engineering, Southeast University, Nanjing 210096, China*

Peng Xu − *State Key Laboratory of Millimeter Waves, School of Information Science and Engineering, Southeast University, Nanjing 210096, China*

Complete contact information is available at:
https://pubs.acs.org/10.1021/acsomega.1c04733

Notes

The authors declare no competing financial interest.

■ REFERENCES

(1) Yu, N.; Genevet, P.; Kats, M. A.; Aieta, F.; Tetienne, J.-P.; Capasso, F.; Gaburro, Z. Light Propagation with Phase Discontinuities: Generalized Laws of Reflection and Refraction. *Science* **2011**, *334*, 333−337.

(2) Yu, N.; Capasso, F. Flat Optics with Designer Metasurfaces. *Nat. Mater.* **2014**, *13*, 139−150.

(3) Grady, N. K.; Heyes, J. E.; Chowdhury, D. R.; Zeng, Y.; Reiten, M. T.; Azad, A. K.; Taylor, A. J.; Dalvit, D. A. R.; Chen, H.-T. Terahertz Metamaterials for Linear Polarization Conversion and Anomalous Refraction. *Science* **2013**, *340*, 1304−1307.

(4) Zhang, X.; Tian, Z.; Yue, W.; Gu, J.; Zhang, S.; Han, J.; Zhang, W. Broadband Terahertz Wave Deflection Based on C-Shape Complex Metamaterials with Phase Discontinuities. *Adv. Mater.* **2013**, *25*, 4567−4572.

(5) Sun, S.; He, Q.; Xiao, S.; Xu, Q.; Li, X.; Zhou, L. Gradient-Index Meta-Surfaces as a Bridge Linking Propagating Waves and Surface Waves. *Nat. Mater.* **2012**, *11*, 426−431.

(6) Yang, Y.; Wang, W.; Moitra, P.; Kravchenko, I. I.; Briggs, D. P.; Valentine, J. Dielectric Meta-Reflectarray for Broadband Linear Polarization Conversion and Optical Vortex Generation. *Nano Lett.* **2014**, *14*, 1394−1399.

(7) Balthasar Mueller, J. P.; Rubin, N. A.; Devlin, R. C.; Groever, B.; Capasso, F. Metasurface Polarization Optics: Independent Phase Control of Arbitrary Orthogonal States of Polarization. *Phys. Rev. Lett.* **2017**, *118*, 113901.

(8) Xu, H.-X.; Han, L.; Li, Y.; Sun, Y.; Zhao, J.; Zhang, S.; Qiu, C.-W. Completely Spin-Decoupled Dual-Phase Hybrid Metasurfaces for Arbitrary Wavefront Control. *ACS Photonics* **2019**, *6*, 211−220.

(9) Ding, G.; Chen, K.; Qian, G.; Zhao, J.; Jiang, T.; Feng, Y.; Wang, Z. Independent Energy Allocation of Dual-Helical Multi-Beams with Spin-Selective Transmissive Metasurface. *Adv. Opt. Mater.* **2020**, *8*, 2000342.

(10) Guo, W.-L.; Wang, G.-M.; Ji, W.-Y.; Zheng, Y.-L.; Chen, K.; Feng, Y. Broadband Spin-Decoupled Metasurface for Dual-Circularly Polarized Reflector Antenna Design. *IEEE Trans. Antennas Propag.* **2020**, *68*, 3534−3543.

(11) Xu, H. X.; Hu, G.; Jiang, M.; Tang, S.; Wang, Y.; Wang, C.; Huang, Y.; Ling, X.; Liu, H.; Zhou, J. Wavevector and Frequency Multiplexing Performed by a Spin-Decoupled Multichannel Metasurface. *Adv. Mater. Technol.* **2020**, *5*, 1900710.

(12) Wang, Z. X.; Wu, J. W.; Wu, L. W.; Gou, Y.; Ma, H. F.; Cheng, Q.; Cui, T. J. High Efficiency Polarization-Encoded Holograms with Ultrathin Bilayer Spin-Decoupled Information Metasurfaces. *Adv. Opt. Mater.* **2021**, *9*, 2001609.

(13) Zhao, R.; Sain, B.; Wei, Q.; Tang, C.; Li, X.; Weiss, T.; Huang, L.; Wang, Y.; Zentgraf, T. Multichannel Vectorial Holographic Display and Encryption. *Light: Sci. Appl.* **2018**, *7*, 95.

(14) Xu, P.; Tian, H. W.; Cai, X.; Jiang, W. X.; Cui, T. J. Radiation-Type Metasurfaces for Advanced Electromagnetic Manipulation. *Adv. Funct. Mater.* **2021**, *31*, 2100569.

(15) Li, Z.; Chen, C.; Guan, Z.; Tao, J.; Chang, S.; Dai, Q.; Xiao, Y.; Cui, Y.; Wang, Y.; Yu, S.; Zheng, G.; Zhang, S. Three-Channel Metasurfaces for Simultaneous Meta-Holography and Meta-Nanoprinting: A Single-Cell Design Approach. *Laser Photonics Rev.* **2020**, *14*, 2000032.

(16) Li, J.; Wang, Y.; Chen, C.; Fu, R.; Zhou, Z.; Li, Z.; Zheng, G.; Yu, S.; Qiu, C. W.; Zhang, S. From Lingering to Rift: Metasurface Decoupling for Near- and Far-Field Functionalization. *Adv. Mater.* **2021**, *33*, 2007507.

(17) Xu, H.-X.; Wang, Y.; Wang, C.; Wang, M.; Wang, S.; Ding, F.; Huang, Y.; Zhang, X.; Liu, H.; Ling, X.; Huang, W. Deterministic approach to achieve full-polarization cloak. *Research* **2021**, *2021*, 6382172.

(18) Li, S.; Wang, Z.; Dong, S.; Yi, S.; Guan, F.; Chen, Y.; Guo, H.; He, Q.; Zhou, L.; Sun, S. Helicity-Delinked Manipulations on Surface Waves and Propagating Waves by Metasurfaces. *Nanophotonics* **2020**, *9*, 3473−3481.

(19) Plum, E.; Zheludev, N. I. Chiral Mirrors. *Appl. Phys. Lett.* **2015**, *106*, 221901.

(20) Wang, Z.; Jia, H.; Yao, K.; Cai, W.; Chen, H.; Liu, Y. Circular Dichroism Metamirrors with Near-Perfect Extinction. *ACS Photonics* **2016**, *3*, 2096−2101.

(21) Jing, L.; Wang, Z.; Maturi, R.; Zheng, B.; Wang, H.; Yang, Y.; Shen, L.; Hao, R.; Yin, W.; Li, E.; Chen, H. Gradient Chiral Metamirrors for Spin-Selective Anomalous Reflection. *Laser Photonics Rev.* **2017**, *11*, 1700115.

(22) Xu, H.-X.; Hu, G.; Li, Y.; Han, L.; Zhao, J.; Sun, Y.; Yuan, F.; Wang, G.-M.; Jiang, Z. H.; Ling, X.; Cui, T. J.; Qiu, C.-W. Interference-Assisted Kaleidoscopic Meta-Plexer for Arbitrary Spin-Wavefront Manipulation. *Light: Sci. Appl.* **2019**, *8*, 3.

(23) Wang, Q.; Plum, E.; Yang, Q.; Zhang, X.; Xu, Q.; Xu, Y.; Han, J.; Zhang, W. Reflective Chiral Meta-Holography: Multiplexing Holograms for Circularly Polarized Waves. *Light: Sci. Appl.* **2018**, *7*, 25.

(24) Wang, L.; Huang, X.; Li, M.; Dong, J. Chirality Selective Metamaterial Absorber with Dual Bands. *Opt. Express* **2019**, *27*, 25983.

(25) Li, Z.; Liu, W.; Cheng, H.; Choi, D. Y.; Chen, S.; Tian, J. Spin-Selective Full-Dimensional Manipulation of Optical Waves with Chiral Mirror. *Adv. Mater.* **2020**, *32*, 1907983.

(26) Jing, L.; Wang, Z.; Yang, Y.; Zheng, B.; Liu, Y.; Chen, H. Chiral Metamirrors for Broadband Spin-Selective Absorption. *Appl. Phys. Lett.* **2017**, *110*, 231103.

(27) Cui, T. J.; Qi, M. Q.; Wan, X.; Zhao, J.; Cheng, Q. Coding Metamaterials, Digital Metamaterials and Programmable Metamaterials. *Light: Sci. Appl.* **2014**, *3*, No. e218.

(28) Wu, R. Y.; Shi, C. B.; Liu, S.; Wu, W.; Cui, T. J. Addition Theorem for Digital Coding Metamaterials. *Adv. Opt. Mater.* **2018**, *6*, 1701236.

(29) Liu, S.; Cui, T. J.; Xu, Q.; Bao, D.; Du, L.; Wan, X.; Tang, W. X.; Ouyang, C.; Zhou, X. Y.; Yuan, H.; Ma, H. F.; Jiang, W. X.; Han, J.; Zhang, W.; Cheng, Q. Anisotropic Coding Metamaterials and

Their Powerful Manipulation of Differently Polarized Terahertz Waves. *Light: Sci. Appl.* **2016**, *5*, No. e16076.

(30) Ma, Q.; Shi, C. B.; Bai, G. D.; Chen, T. Y.; Noor, A.; Cui, T. J. Beam-Editing Coding Metasurfaces Based on Polarization Bit and Orbital-Angular-Momentum-Mode Bit. *Adv. Opt. Mater.* **2017**, *5*, 1700548.

(31) Liu, S.; Zhang, H. C.; Zhang, L.; Yang, Q. L.; Xu, Q.; Gu, J.; Yang, Y.; Zhou, X. Y.; Han, J.; Cheng, Q.; Zhang, W.; Cui, T. J. Full-State Controls of Terahertz Waves Using Tensor Coding Metasurfaces. *ACS Appl. Mater. Interfaces* **2017**, *9*, 21503−21514.

(32) Liu, S.; Zhang, L.; Yang, Q. L.; Xu, Q.; Yang, Y.; Noor, A.; Zhang, Q.; Iqbal, S.; Wan, X.; Tian, Z.; Tang, W. X.; Cheng, Q.; Han, J. G.; Zhang, W. L.; Cui, T. J. Frequency-Dependent Dual-Functional Coding Metasurfaces at Terahertz Frequencies. *Adv. Opt. Mater.* **2016**, *4*, 1965−1973.

(33) Wu, H.; Liu, S.; Wan, X.; Zhang, L.; Wang, D.; Li, L.; Cui, T. J. Controlling Energy Radiations of Electromagnetic Waves via Frequency Coding Metamaterials. *Adv. Sci.* **2017**, *4*, 1700098.

(34) Chen, L.; Ma, Q.; Nie, Q. F.; Hong, Q. R.; Cui, H. Y.; Ruan, Y.; Cui, T. J. Dual-Polarization Programmable Metasurface Modulator for near-Field Information Encoding and Transmission. *Photonics Res.* **2021**, *9*, 116.

(35) Ma, Q.; Bai, G. D.; Jing, H. B.; Yang, C.; Li, L.; Cui, T. J. Smart Metasurface with Self-Adaptively Reprogrammable Functions. *Light: Sci. Appl.* **2019**, *8*, 98.

(36) Ma, Q.; Hong, Q. R.; Gao, X. X.; Jing, H. B.; Liu, C.; Bai, G. D.; Cheng, Q.; Cui, T. J. Smart sensing Metasurface with self-Defined Functions in Dual Polarizations. *Nanophotonics* **2020**, *9*, 3271−3278.

(37) Zhang, L.; Liu, S.; Li, L.; Cui, T. J. Spin-Controlled Multiple Pencil Beams and Vortex Beams with Different Polarizations Generated by Pancharatnam-Berry Coding Metasurfaces. *ACS Appl. Mater. Interfaces* **2017**, *9*, 36447−36455.

(38) Ding, G.; Chen, K.; Luo, X.; Zhao, J.; Jiang, T.; Feng, Y. Dual-Helicity Decoupled Coding Metasurface for Independent Spin-to-Orbital Angular Momentum Conversion. *Phys. Rev. Appl.* **2019**, *11*, 044043.

(39) Bai, G. D.; Ma, Q.; Li, R. Q.; Mu, J.; Jing, H. B.; Zhang, L.; Cui, T. J. Spin-Symmetry Breaking Through Metasurface Geometric Phases. *Phys. Rev. Appl.* **2019**, *12*, 044042.

(40) Bai, G. D.; Cui, T. J. Representing Quantum Information with Digital Coding Metasurfaces. *Adv. Sci.* **2020**, *7*, 2001648.